

## Research Paper

# Visualization of Macrophage Recruitment to Inflammation Lesions using Highly Sensitive and Stable Radionuclide-Embedded Gold Nanoparticles as a Nuclear Bio-Imaging Platform

Sang Bong Lee<sup>1,2\*</sup>, Ho Won Lee<sup>1\*</sup>, Thoudam Debraj Singh<sup>1</sup>, Yinghua Li<sup>3</sup>, Sang Kyoong Kim<sup>9</sup>, Sung Jin Cho<sup>4</sup>, Sang-Woo Lee<sup>1,2</sup>, Shin Young Jeong<sup>1</sup>, Byeong-Cheol Ahn<sup>1</sup>, Sangil Choi<sup>5</sup>, In-Kyu Lee<sup>2,6</sup>, Dong-Kwon Lim<sup>7</sup>✉, Jaetae Lee<sup>1,8</sup>✉, Yong Hyun Jeon<sup>2,9</sup>✉

1. Department of Nuclear Medicine, Kyungpook National University Hospital, Daegu, South Korea;
2. Leading-edge Research Center for Drug Discovery and Development for Diabetes and Metabolic Disease, Kyungpook National University Hospital, Daegu, South Korea;
3. Department of Pathology, Chemon Co. Ltd., 240, Nampyeong-Ro, Yangji-Myeon, Cheoin-Gu, Yongin-Si, Gyeonggi-Do, 17162, Republic of Korea;
4. New Drug Development Center, Daegu-Gyeongbuk Medical Innovation Foundation, Daegu, South Korea;
5. Department of Pharmacy, School of Pharmacy, Massachusetts College of Pharmacy and Health Sciences, Boston, Massachusetts, USA;
6. Department of Internal Medicine, Kyungpook National University School of Medicine, Daegu 700-721, South Korea;
7. KU-KIST Graduate School of Converging Science and Technology, Korea University, Seoul Anam-ro 145, South Korea;
8. Daegu-Gyeongbuk Medical Innovation Foundation, Daegu, South Korea;
9. Laboratory Animal Center, Daegu-Gyeongbuk Medical Innovation Foundation, Daegu, South Korea.

\*The first two authors contributed equally to this study.

✉ Corresponding authors: Yong Hyun Jeon (jeong9014@gmail.com), Jaetae Lee (jaetae@knu.ac.kr), and Dong-Kwon Lim (dklim@korea.ac.kr).

© Ivyspring International Publisher. This is an open access article distributed under the terms of the Creative Commons Attribution (CC BY-NC) license (<https://creativecommons.org/licenses/by-nc/4.0/>). See <http://ivyspring.com/terms> for full terms and conditions.

Received: 2016.08.07; Accepted: 2016.12.08; Published: 2017.02.12

## Abstract

Reliable and sensitive imaging tools are required to track macrophage migration and provide a better understating of their biological roles in various diseases. Here, we demonstrate the possibility of radioactive iodide-embedded gold nanoparticles (RIe-AuNPs) as a cell tracker for nuclear medicine imaging. To demonstrate this utility, we monitored macrophage migration to carrageenan-induced sites of acute inflammation in living subjects and visualized the effects of anti-inflammatory agents on this process. Macrophage labeling with RIe-AuNPs did not alter their biological functions such as cell proliferation, phenotype marker expression, or phagocytic activity. *In vivo* imaging with positron-emission tomography revealed the migration of labeled macrophages to carrageenan-induced inflammation lesions 3 h after transfer, with highest recruitment at 6 h and a slight decline of radioactive signal at 24 h; these findings were highly consistent with the data of a bio-distribution study. Treatment with dexamethasone (an anti-inflammation drug) or GSK5182 (an ERRγ inverse agonist) hindered macrophage recruitment to the inflamed sites. Our findings suggest that a cell tracking strategy utilizing RIe-AuNPs will likely be highly useful in research related to macrophage-related disease and cell-based therapies.

Key words: gold nanoparticles, nuclear bio-imaging platform, macrophage migration, acute inflammation.

## Introduction

Cell labeling and tracking represent an essential factor toward obtaining a better understanding of complex biological mechanisms and investigating the therapeutic effects of infused cells in a living organism

[1, 2]. Through various *in vivo* imaging agents, the direct labeling of cells of interest such as macrophages [3], dendritic cells [4], and stem cells [5, 6] enables us to monitor the fate of infused cells and evaluate their

functional effects in the microenvironments associated with various diseases.

Macrophages are among the several types of immune cells that play numerous roles in inflammation, allergies, diabetes, infection, and cancer [7]. Thus, it is essential to monitor their biological behaviors in the complex circumstances of inflammatory disease to discover therapeutic strategies for controlling such disorders.

Many studies have accomplished the visualization of macrophage migration *in vivo* through the use of various molecular imaging strategies including fluorescent imaging [8], positron emission tomography (PET)/single photon emission computer tomography imaging [9, 10], magnetic resonance imaging (MRI) [11], and multimodal imaging [12] (cf. MRI plus photoacoustic imaging) via indirect and direct methods. Among these, nuclear medicine imaging is utilized in the clinical setting owing to its excellent penetration, sensitivity, and capability for quantitative analysis. To facilitate the sensitive and quantitative tracking of macrophage recruitment using nuclear medicine imaging, the development of highly sensitive and stable imaging probes is required to distinguish the small population of macrophages that have migrated into the inflamed lesion from the high background activity that originates from physiological uptake of the surrounding tissue.

Recently, we have developed radioactive iodide-encapsulated gold nanoparticle probes (RIe-AuNPs) for a novel nuclear medicine imaging platform that features a simple and straightforward approach [13]. As these imaging agents exhibit marked sensitivity and stability in living mice, they might facilitate the early detection of macrophage migration to inflamed lesions as well as the serial monitoring of systemic distribution to various organs in response to inflammation stimuli, with associated easy and rapid quantification based on computed tomography (CT) segmentation.

Here, we attempted to track macrophage migration to carrageenan-induced acute inflammatory sites in living mice and to monitor the therapeutic outcomes of anti-inflammatory agents on this process through the use of highly sensitive and stable RIe-AuNPs as a cell tracking system for nuclear medicine imaging.

## Materials and Methods

### Synthesis of RIe-AuNPs

Detailed procedures for the synthesis of RIe-AuNPs are described in the supplementary materials.

### Cell labeling with RIe-AuNPs

Primary peritoneal macrophages were prepared using our previously published methods<sup>3</sup>. RIe-AuNPs (2 nM) were added to the macrophages and incubated for three hours. The labeling was completed by washing the labeled cells twice with medium and the efficiency of cellular labeling was confirmed using a dose calibrator.

### Cell proliferation assay

Both unlabeled and labeled macrophages were seeded in 96-well flat-bottom plates. After labeling, 10  $\mu$ L CCK-8 solution was supplemented to the respective wells, followed by further incubation at 37°C for three hours. The absorbance at 450 nm was determined using a plate reader (BMG Labtech, Offenburg, Germany).

### Phagocytic activity assay

The phagocytic ability of macrophages was assessed using previously reported methods [14]. Detail procedures are described in the supplementary materials.

### Animal studies

*Study 1.* The abbreviated scheme for *in vivo* macrophage tracking is illustrated in Fig. S7. Briefly, RIe-AuNP-labeled macrophages ( $3 \times 10^6$  cells) were intravenously administered to animals (7 mice). At day 1 after injection, baseline activity of radionuclides was acquired prior to the induction of inflammation. For inflammation induction, PBS and 1% carrageenan (CG) solution were administered to the respective footpads. PET scans were performed at the indicated time points. After twenty-four hours, footpads were excised, followed by *ex vivo* imaging.

*Study 2.* The experimental scheme for the drug intervention study is described in Fig. S9. At day 1 after the injection of labeled macrophages, mice were divided into three groups: vehicle, dexamethasone (DEX), and GSK5182 groups (7 mice/group). Inflammatory stimuli were generated using the same procedure as described above. Either a single dose of 10 mg/kg DEX, GSK5182, or vehicle was administered to an animal with inflammation after inflammation induction. PET was conducted to determine the recruitment of macrophages at the indicated times.

### In vivo PET/CT study

For the PET/computer tomography (CT) study, a 20 minute scan (tumor imaging) was performed using LabPET8 (TriFoil Imaging, Waukesha, WI). For <sup>18</sup>F-FDG PET/CT imaging, a 10 minute scan was performed using the same animal PET/CT

instrument. CT scans were conducted after the PET scan. Detail procedures for PET/CT imaging are described in the supplementary materials.

### Bio-distribution study

Mice (7 mice/group) were sacrificed at 0, 3, 6, and 24 hours after the injection of macrophages. The excised organs were weighed and the radioactivity of each organ was measured using a  $\gamma$  counter.

## Results and Discussion

### Rle-AuNP characterization and macrophage labeling

Previously, we successfully established highly sensitive and stable imaging agents as a nuclear medicine imaging platform (RIe-AuNPs) [13]. Briefly, 20 nm core gold nanoparticles (AuNPs) were first functionalized with thiolated adenine bases ( $A_{10}$ ), which allow for radio-labeling of over 2700 radioactive iodine molecules ( $Na^{124}I$  or  $Na^{125}I$ ) on each adenine-rich-DNA-modified gold nanoparticle ( $A_{10}$ -AuNP) (Fig. 1a). The labeling of radioiodine on  $A_{10}$ -AuNPs was rapidly completed within 120 min post-reaction (Fig. S1) at room temperature (RI-AuNPs). Furthermore, we assessed whether

differences of labeling kinetics and efficiency could be identified between  $Na^{124}I$  or  $Na^{125}I$  on  $A_{10}$ -AuNPs. As shown in Fig. S2, no differences of labeling kinetics and efficiency were found between the two different types of radioactive iodides. Next, the additional gold shell was produced to create RIe-AuNPs, which can substantively increase their *in vivo* stability. UV-visible spectra of RIe-AuNPs showed characteristic extinction spectra in the visible region, representing the lack of particle aggregation (Fig. S3a). X-ray photoelectron spectroscopy (XPS) analysis clearly revealed the existence of Au (4f, 4p<sup>1</sup>) and iodine (3d<sup>5</sup>) in the RIe-AuNPs (Fig. S3b). Furthermore, the core and shell structure with a round shape was visible in transmission electron microscopy analysis as shown in Fig. 1b and energy dispersive spectroscopy also indicated the existence of iodine surrounding the core gold nanoparticles (Fig. 1b). Finally, the stability of the radioactive iodide on nanoparticles is an important factor for biomedical imaging. When we examined the stability of RIe-AuNPs in human serum, they exhibited marked stability without any release of radionuclide from the RIe-AuNPs (Fig. S4), unlike that observed for RI-AuNPs (without the gold shell).

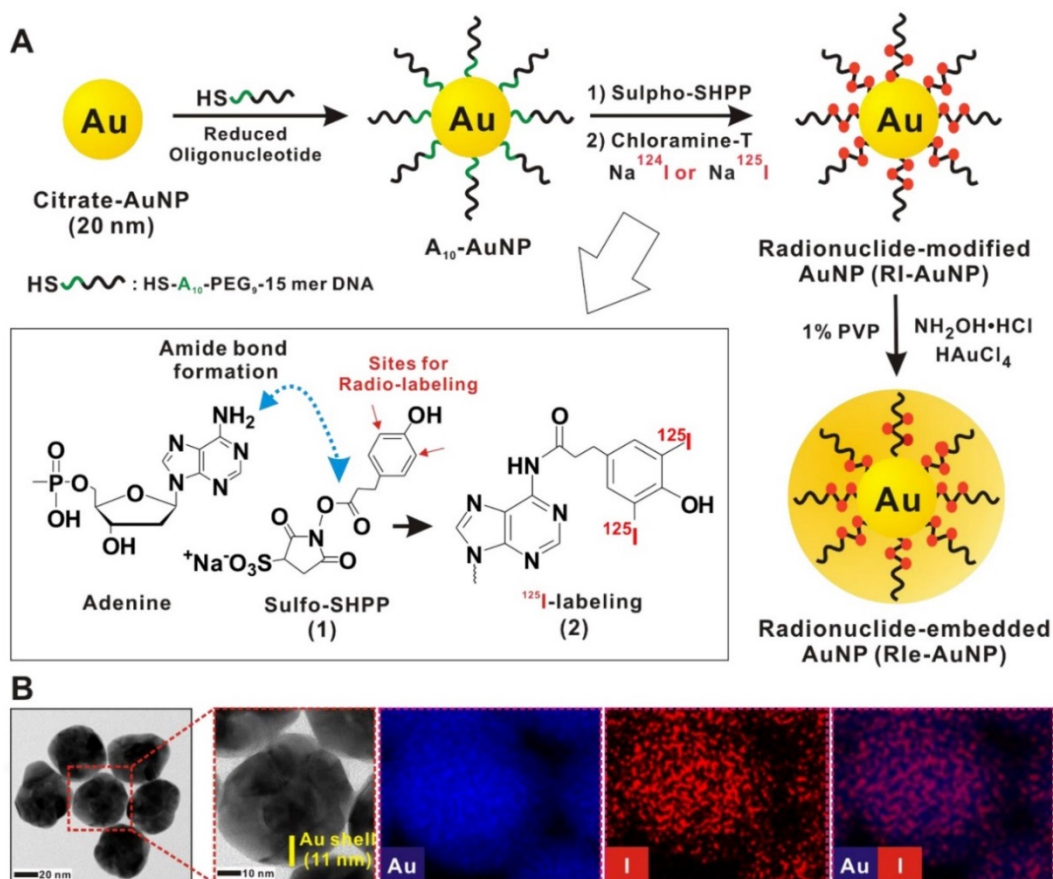


**Figure 1.** Schematic procedure of Rle-AuNP synthesis. (a) Schematic of Rle-AuNP synthesis. (b) High resolution transmission electron microscope images as well as energy-dispersive X-ray analysis of Rle-AuNPs. Blue and red indicate gold and iodine, respectively.

The main difference of our probe design compared with that of other probes should be noted. Numerous other reports have shown the labeling strategy of bonding radioiodine onto gold nanoparticles through direct incorporation [15-21]. However, these methods allow only a small number of radioiodine labels to be incorporated on AuNPs; in addition, maintaining the stability of labeled radioiodine remains challenging within *in vivo* environments. For example, the probe in the report of Kim et al. [15] utilized citrate-modified AuNPs with NaI conjugated on the surface of the AuNPs through Au-I bonds (yielding only 6 iodine molecules per AuNP), following which mPEG thiol was used to generate stable AuNPs under physiological conditions. In contrast, the radio-isotope conjugation in the current work differs completely from that reported by Kim et al. [15]. Instead, we utilized adenine-rich thiolated oligonucleotide modified AuNPs as a core, then we covalently labeled radio-isotopes with the DNA base (adenine), and finally we produced an additional Au shell to yield radio-isotope embedded Au-Au core shell nanostructures. Thus, based on these improvements of our probe design, a highly sensitive and stable imaging probe could be produced for use in a living organism.

Promising cell-labeling agents should guarantee easy, efficient, as well as stable labeling [1]. Macrophages exhibit robust phagocytosis that consumes all kinds of tiny particles [22]. Therefore, macrophages are able to be simply tagged with RIe-AuNPs. The labeling efficiency of the RIe-AuNPs into the macrophages increased in a particle dose-dependent manner (1.0-8.0 nM), with uptake efficiency reaching a peak at 2 nM RIe-AuNPs (Fig.

2a). Microscopy imaging clearly showed the presence of RIe-AuNPs in labeled but not unlabeled macrophages (Fig. 2b). For long-term, sensitive, and quantitative trafficking of macrophages *in vivo*, imaging agents should be retained in the cells for long time periods. As illustrated in Fig. 2c, over 75% of the initial radioactivity was maintained in labeled macrophages even after 2 days, even though the radioactivity of the imaging particles in labeled cells was slightly decreased. In contrast, after incubation for 3 hours, RI-AuNPs (without gold shells) in macrophages revealed a rapid reduction of radioactivity owing to the absence of a protective layer (Fig. S5). To further demonstrate the stability of our imaging platform *in vivo*, the biodistribution of RIe-AuNPs was investigated following intravenous injection of particles. RIe-AuNPs were administered intravenously to mice and then PET/CT imaging as well as biodistribution analyses were conducted at the indicated times after injection. As a result, we could observe strong accumulation of RIe-AuNPs in the liver at 1 and 24 hours after injection (Fig. S6a and S6b), which is consistent with the biodistribution results (Fig. S6c). Furthermore, whereas we were unable to detect the radioactive signal in the thyroid using the PET detector because of weak radioactive signals, the biodistribution data showed that the thyroid exhibited the lowest uptake of injected RIe-AuNPs; which might instead have resulted from the physiological uptake of a few radioiodine molecules that had been cleaved from the nanoparticles, suggesting that these particles exhibit excellent stability *in vivo*. The results thus indicate the excellent stability of the RIe-AuNPs in macrophages as well as *in vivo* in an organism, effected by the efficient protection from the Au shell.

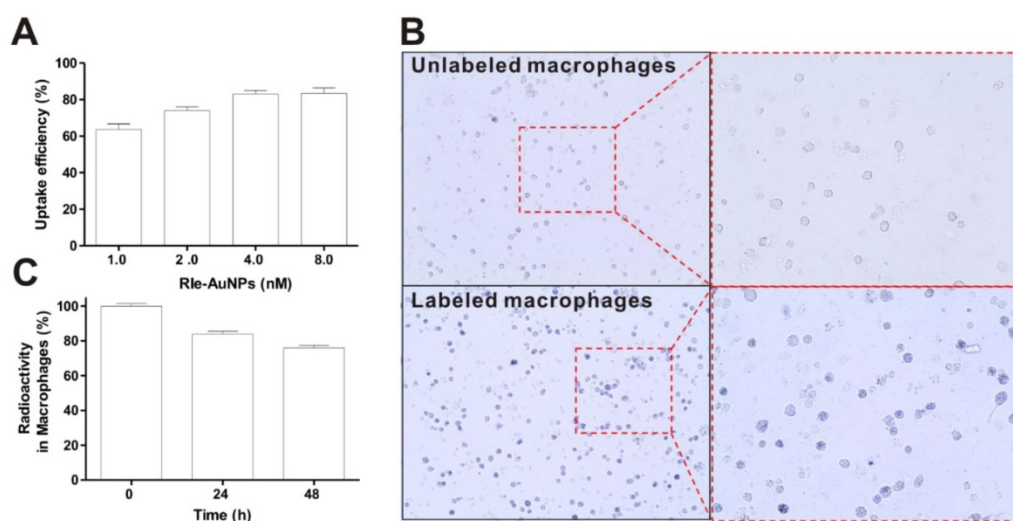


**Figure 2.** Cellular labeling of RIe-AuNPs. (a) Cellular uptake of various doses of RIe-AuNPs. (b) Bright-field photographs of macrophages after cell labeling with RIe-AuNPs (2 nM). (c) Residual radioactivity in macrophages over time.

## Effect of cell labeling on biological functions of macrophages

For successful application of imaging agents to *in vivo* cell tracking, the viability and function of the cells of interest should not be altered after cell labeling. Therefore, we examined whether the labeling of R1e-AuNPs affects macrophage cell proliferation and function.

The results of a cell proliferation assay using CCK-8 agents showed no differences between unlabeled and labeled macrophages until 48 hours (Fig. 3a). Furthermore, the particles did not lead to cellular apoptosis, as determined by cell labeling of Annexin V and PI staining (data not shown). Macrophage phenotype markers were next evaluated using macrophage specific markers (CD86, CD11b, and F4/80 antibodies). We could observe the high expression of these markers in macrophages (Fig. 3b and Fig. S7). In contrast, the gene expression of CD4, a helper T-lymphocyte marker, was not visible in unlabeled or labeled cells. To determine whether phagocytic activity differed between unlabeled and labeled macrophages, the cells were co-incubated with 7-AAD-tagged bacteria at 4°C or 37°C. As shown in Fig. 3c, no difference of phagocytic activity was exhibited between the two groups. The percentage of unlabeled and labeled cells was  $55.9 \pm 4.2$  and  $54.07 \pm 5.1\%$ , respectively. Conversely, phagocytic activity was completely inhibited at 4°C in both macrophage groups ( $10.7 \pm 0.9$  and  $11.2 \pm 1.3\%$ ). These results suggest that R1e-AuNPs represent biocompatible imaging agents for *in vivo* macrophage tracking without concomitant alternation of macrophage cellular function.

## Tracking of macrophage recruitment to acute inflammatory sites by PET/CT

*In vivo* macrophage tracking was conducted to demonstrate the potential for R1e-AuNPs to serve as an *in vivo* cell tracker (Fig. S8). For the tracking of macrophage migration to inflammation lesions, a CG-induced acute inflammation model was adopted in immunocompetent mice. Carrageenan has previously been utilized to induce acute inflammation in murine models [23]. In turn, [<sup>18</sup>F]FDG-PET has been applied to evaluate inflammation levels in living subjects [24]. When we monitored the mice with CG-induced acute inflammation via [<sup>18</sup>F] FDG PET/CT, we detected a strong uptake of radiotracer at inflamed lesions (Fig. S9).

The distribution of labeled macrophages in the lung, liver, and spleen was observed at 24 hours post-transfer (Fig. 4a-Baseline) by PET scan. At 3 hours post-inflammation induction, the recruitment of macrophages to the inflammatory sites was first detected and this migration peaked at 6 hours (Fig. 4a and 4b). But, we cannot observe difference of radioactivity between inflamed footpads and control footpads at 24 hours. Excised footpads also showed distinct radioactive signals in CG- but not PBS-injected footpads (Fig. 4c, 6h after induction of inflammation). In order to verify the PET signal, we assessed the levels of inflammatory biomarkers such as IL- $\beta$ , IL-6, and TNF- $\alpha$  at the inflammatory lesions through the use of real-time PCR with total RNA isolated from CG- or PBS-injected footpads. Consistent with the PET signals, we determined that the levels of pro-inflammatory cytokines were much higher in the CG-injected than PBS-injected footpads (Fig. S10).

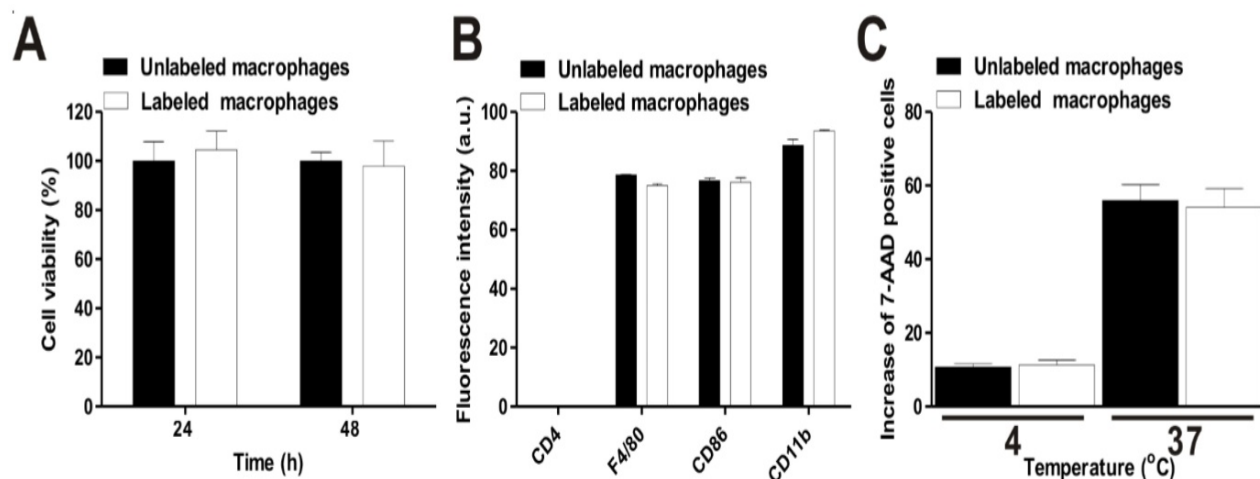


**Figure 3.** Effects of cell labeling with R1e-AuNPs on the biological functions of macrophages. (a) Viability of macrophages (black bar: unlabeled; empty bar: labeled). (b) Phenotype marker analysis (negative: CD4, macrophage-specific: F4/80, CD86, and CD11b) of unlabeled (black bar) and labeled (empty bar) macrophages. (c) Phagocytic activity of macrophages; black and empty bars indicate unlabeled and labeled cells, respectively.

The data of bio-distribution analysis were also consistent with those of PET imaging. The majority of infused macrophages remained in the liver and lung. Approximately 0.8–1.0% of the macrophages migrated to the inflamed lesion (Fig. 4d and e), with peak migration at 6 hours post-inflammation induction. Notably, despite the large number ( $3 \times 10^6$ ) of injected macrophages, we could detect only a small migrated population at the inflamed lesion by PET imaging. Previously, reports from Ren et al. [25] have demonstrated the level of macrophage recruitment to the inflamed lesion (simplex bone cement-induced inflammation) from day 4 after inflammation induction using a luciferase reporter gene as a highly sensitive reporter; however, it was impossible to

detect their migration to the inflamed site as early as 24 hours owing to the low number of infiltrated macrophages. More recently, Wattananit et al. [26] have demonstrated that only six thousand cells could be detected in an inflammation lesion (stroke area) among  $4 \times 10^6$  i.v.-injected GFP+ monocytes by quantitative immunohistochemical analysis. Therefore, considering the small population of infused cells that successfully migrate into the inflamed lesion, our findings emphasize the high sensitivity and considerable potential of our imaging platform, which allows us to enable the monitoring of *in vivo* biological behavior of a small population of macrophages.

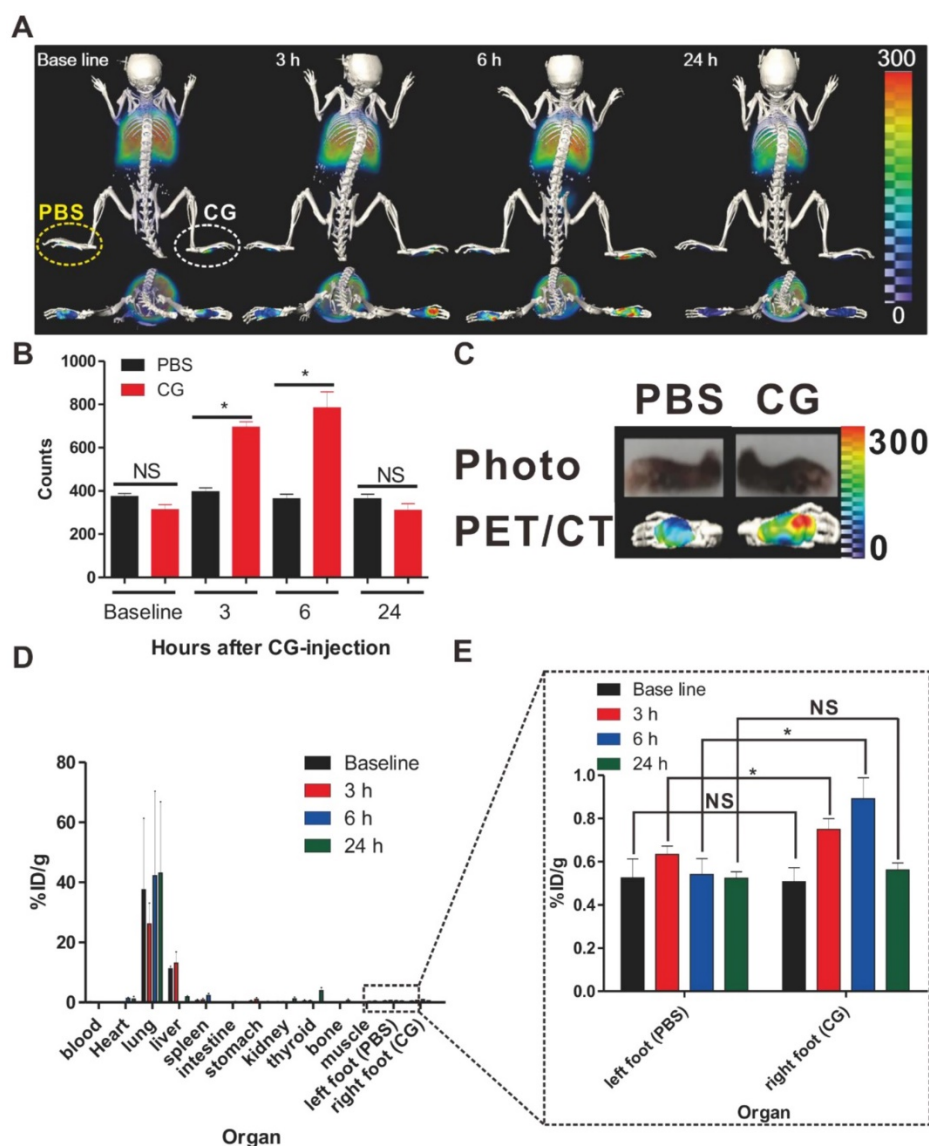


**Figure 4.** PET/CT imaging of macrophage migration to inflamed lesions. (a) 3D-PET/CT images and transverse PET/CT images over time. The yellow and white circles indicate the PBS- and CG-injected footpads, respectively. (b) Region of interest (ROI) analysis to determine the radioactivity in the footpads. Data represent the means  $\pm$  standard deviations (SDs),  $n = 7$ . (c) *Ex vivo* PET/CT images of excised footpads at 6h. (d) Time-dependent bio-distribution of labeled macrophages in whole organs post-transfer. (e) The black box shows the enlarged data to clearly reveal the changes of radioactivity in CG-injected footpads. %ID/g represents percentage injected dose per gram. \* $P < 0.05$ , NS; not significant.

We further examined the presence of infiltrated macrophage in CG-injected footpads by immunohistological analysis. Gold particles localized in various tissues are usually seen as dark color particles by hematoxylin and eosin (H&E) staining analysis. As seen in Fig. S11, we could observe dark color particle-containing macrophages in CG-injected footpads by histological analysis based on H&E staining; furthermore, their number was highest at 6 hours after CG-injection, which is consistent with the PET signal. However, no dark particle-containing macrophages were observed in the PBS-injected footpads.

Additionally, the issue of biocompatibility/toxicity is very important for the further application of R1e-AuNPs to both preclinical and clinical situations. To evaluate this concern, we determined whether R1e-AuNPs induce toxicity *in vivo* by histological analysis using H&E staining. Histopathologic analysis of major organs such as the liver, spleen, and kidney did not reveal any significant histopathological abnormalities in either normal mice or mice receiving R1e-AuNP-labeled macrophages until 14 days post-transfer (Fig. S12). However, although no adverse effects of R1e-AuNPs were observed *in vivo*, further extensive studies should be required to evaluate the acute and chronic toxicity of R1e-AuNPs after systemic administration prior to their clinical application.

These results indicate that R1e-AuNPs represent promising nuclear imaging agents for the evaluation of *in vivo* biological behavior in an acute inflammation disease model.

### **Assessment of the effects of anti-inflammation agents on R1e-AuNP-labeled macrophage migration to inflammatory lesions using established macrophage-tracking strategies with R1e-AuNPs**

Next, we attempted to determine whether our macrophage tracking approach exhibited marked potential to investigate the therapeutic outcomes of anti-inflammatory or new candidate agents in living subjects with inflammation. Two kinds of drugs, DEX and GSK5182, were used for this study. DEX, as a type of steroid medication, has been demonstrated to inhibit inflammation [27]. GSK5182 is an inverse agonist for estrogen-related receptor gamma (ERR $\gamma$ ) that is in the orphan nuclear receptor family. It has been found that ERR $\gamma$  has essential roles for cell homeostasis and development [28-30]. Although several reports have demonstrated that GSK5182 exhibits therapeutic efficacy against inflammation-

related conditions such as diabetes and microbial infection, no studies have examined the anti-inflammatory effects of GSK5182 against acute inflammation. Therefore, to evaluate the therapeutic efficacy of the respective drugs against acute inflammation, labeled macrophages were transferred to mice and then CG-induced inflammation was generated after 24 h (Fig. S13). Mice received DEX or GSK5182 intraperitoneally immediately after inflammation induction. As shown in Fig. 5a-c, *in vivo* PET/CT imaging clearly demonstrated the marked inhibition of labeled macrophage recruitment to the inflammation sites in the DEX- (Fig. 5a-[2]) and GSK5182 (Fig. 5a-[3])-treated mice at 6 hours after inflammation stimuli. In contrast, the migration of labeled macrophages was obviously shown at site of inflammation in the control mice (Fig. 5a-[1] and 5b-3). Furthermore, consistent with the data of PET imaging, the measurement of dorsoventral thickness of the middle portions of the hind paws, which is a standard method for evaluation of the therapeutic efficiency of anti-inflammation drugs, showed a marked inhibition of paw edema in DEX- or GSK5182-treated mice but not in vehicle-treated mice (Fig. S14). These results suggest that R1e-AuNPs are valuable biomaterials for the evaluation of anti-inflammatory drugs in living mice through the direct macrophage labeling approach.

### **Conclusion**

In summary, the labeling of R1e-AuNPs does not induce adverse effects on macrophage function, including cell proliferation, phenotype marker expression, and phagocytic activity. Notably, the recruitment of primary macrophages to the site of inflammation was successfully visualized via PET/CT imaging using highly sensitive and stable R1e-AuNPs in living mice. Furthermore, the inhibitory effects of DEX, a potent drug against inflammation, as well as of GSK5182, an inverse agonist of ERR $\gamma$ , on macrophage recruitment to the site of inflammation were also demonstrated, suggesting not only that macrophage tracking strategies with R1e-AuNPs represent useful tools to investigate the therapeutic outcome of anti-inflammatory agents but also that ERR $\gamma$  is a promising target for drug discovery in inflammation disease.

### **Supplementary Material**

Supplementary figures and methods.

<http://www.thno.org/v07p0926s1.pdf>

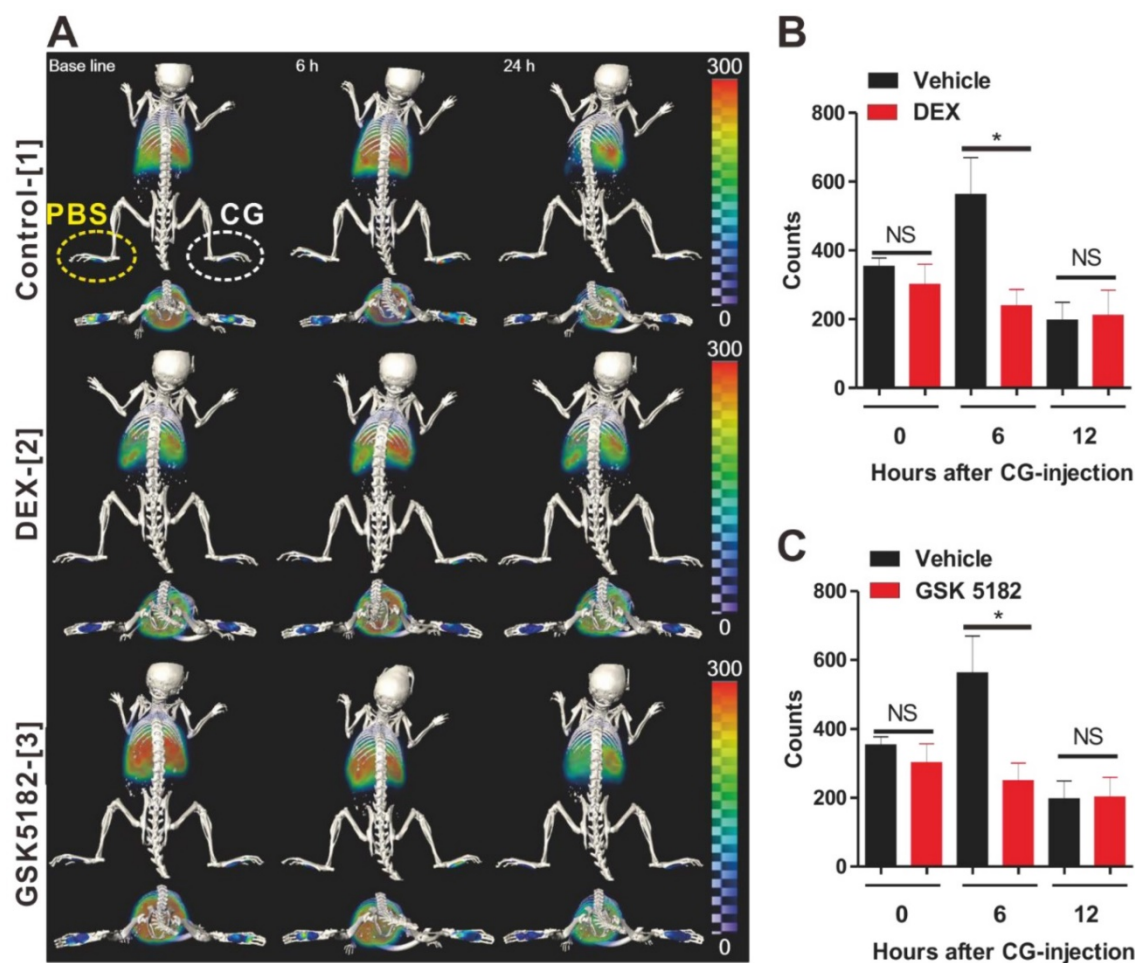


**Figure 5.** Assessments of the therapeutic outcomes of anti-inflammation drugs by the use of cell tracking technique with R1e-AuNPs. (a) 3D-PET/CT image of macrophage migration and axial PET/CT in vehicle-, DEX-, and GSK5182-treated mice. The yellow and white circles indicate the PBS- and CG-injected footpads, respectively. Region of interest analysis of PBS- or CG-injected footpads in (b) DEX-treated mice and (c) GSK5182-treated mice.  $n = 7$ . \* $P < 0.05$ , NS; not significant.

## Abbreviations

AuNPs: gold nanoparticles; CT: computer tomography; DEX: dexamethasone; DTT: dithiothreitol; ERR $\gamma$ R: estrogen-related receptor gamma; FBS: fetal bovine serum; H&E: hematoxylin and eosin; MRI: magnetic resonance imaging; PET: positron emission tomography; R1e-AuNPs: radioactive iodide-embedded gold nanoparticles; XPS: X-ray photoelectron spectroscopy.

## Acknowledgments

This work was supported by a National Research Foundation of Korea (NRF) grant funded by the Korean government (MSIP) (No.2009-0078222, 2009-0078234), a grant of the Korea Health Technology R&D Project through the Korea Health Industry Development Institute (KHIDI), funded by the Ministry of Health & Welfare, Republic of Korea (Grant Number : HI16C1501), the National Nuclear R&D Program through the National Research Foundation of Korea(NRF) funded by the Ministry of

Education, Science and Technology (No.2012M2A2A7014020), a grant from the Medical Cluster R&D Support Project through the Daegu-Gyeongbuk Medical Innovation Foundation (DGMIF), funded by the Ministry of Health & Welfare (grant number: HT13C0002), the BK21 PlusKNU Biomedical Convergence Program, Department of Biomedical Science, Kyungpook National University, a National Research Foundation of Korea (NRF) Grant funded by the Korea Government(MSIP) (No.2014R1A1A1003323), a grant of the Korea Health Technology R&D Project through the Korea Health Industry Development Institute (KHIDI), funded by the Ministry of Health & Welfare (grant number: HI15C0001), a grant of the Medical Cluster R&D support project through the Daegu-Gyeongbuk Medical Innovation Foundation (DGMIF), funded by the Ministry of Health & Welfare, Republic of Korea (grant number: HT15c0003), the Radiation Technology R&D program through the National Research Foundation of Korea funded by the Ministry of Science, ICT & Future Planning

(NRF-2012M2A2A7013480), and a National Research Foundation of Korea (NRF) grant funded by the Korean government (MSIP) (No. NRF-2015M2A2A7A01045177), and NRF-2016R1A2B3013825 (KU-KIST research fund).

## Competing Interests

The authors have declared that no competing interest exists.

## References

- Weissleder R, Nahrendorf M, Pittet MJ. Imaging macrophages with nanoparticles. *Nat Mater.* 2014; 13(2): 125-38.
- Rogers WJ, Meyer CH, Kramer CM. Technology insight: in vivo cell tracking by use of MRI. *Nat. Clin. Pract. Cardiovasc. Med.* 2006; 3(10): 554-62.
- Cai Q-Y, Lee H, Kim E-J, Moon H, Chang K, Rho J, et al. Magnetic resonance imaging of superparamagnetic iron oxide-labeled macrophage infiltrates in acute-phase renal ischemia-reperfusion mouse model. *Nanomedicine.* 2012; 8(3): 365-73.
- Cho N-H, Cheong T-C, Min JH, Wu JH, Lee SJ, Kim D, et al. A multifunctional core-shell nanoparticle for dendritic cell-based cancer immunotherapy. *Nature nanotechnology.* 2011; 6: 675-82.
- Hsiao JK, Tsai CP, Chung TH, Hung Y, Yao M, Liu HM, et al. Mesoporous silica nanoparticles as a delivery system of gadolinium for effective human stem cell tracking. *Small.* 2008; 4(9): 1445-52.
- Lee JM, Kim B-S, Lee H, Im G-I. In vivo tracking of mesenchymal stem cells using fluorescent nanoparticles in an osteochondral repair model. *Mol. Ther.* 2012; 20(7): 1434-42.
- Burke B, Sumner S, Maitland N, Lewis C. Macrophages in gene therapy: cellular delivery vehicles and in vivo targets. *J. Leukoc. Biol.* 2002; 72(3): 417-28.
- Eisenblätter M, Ehrchen J, Varga G, Sunderkötter C, Heindel W, Roth J, et al. In vivo optical imaging of cellular inflammatory response in granuloma formation using fluorescence-labeled macrophages. *J. Nucl. Med.* 2009; 50(10): 1676-82.
- Nahrendorf M, Zhang H, Hembrador S, Panizzi P, Sosnovik DE, Aikawa E, et al. Nanoparticle PET-CT imaging of macrophages in inflammatory atherosclerosis. *Circulation.* 2008; 117: 379-87.
- Pérez-Medina C, Tang J, Abdel-Atti D, Hogstad B, Merad M, Fisher EA, et al. PET imaging of tumor-associated macrophages with <sup>89</sup>Zr-labeled high-density lipoprotein nanoparticles. *J. Nucl. Med.* 2015; 56(8): 1272-7.
- Lee JS, Kang HJ, Gong G, Jung H-D, Lim KH, Kim ST, et al. MR Imaging of in Vivo Recruitment of Iron Oxide-labeled Macrophages in Experimentally Induced Soft-Tissue Infection in Mice. *Radiology.* 2006; 241(1): 142-8.
- Qin H, Zhou T, Yang S, Chen Q, Xing D. Gadolinium (III)-gold nanorods for MRI and photoacoustic imaging dual-modality detection of macrophages in atherosclerotic inflammation. *Nanomedicine.* 2013; 8(10): 1611-24.
- Lee SB, Ahn SB, Lee S-W, Jeong SY, Ghilsuk Y, Ahn B-C, et al. Radionuclide-embedded gold nanoparticles for enhanced dendritic cell-based cancer immunotherapy, sensitive and quantitative tracking of dendritic cells with PET and Cerenkov luminescence. *NPG Asia Mater.* 2016; 8: e281.
- Seo JH, Jeon YH, Lee YJ, Yoon GS, Won D-I, Ha J-H, et al. Trafficking macrophage migration using reporter gene imaging with human sodium iodide symporter in animal models of inflammation. *J. Nucl. Med.* 2010; 51(10): 1637-43.
- Kim YH, Jeon J, Hong SH, Rhim WK, Lee YS, Youn H, et al. Tumor Targeting and Imaging Using Cyclic RGD-PEGylated Gold Nanoparticle Probes with Directly Conjugated Iodine-125. *Small.* 2011; 7(14): 2052-60.
- Jang B, Park S, Kang SH, Kim JK, Kim S-K, Kim I-H, et al. Gold nanorods for target selective SPECT/CT imaging and photothermal therapy in vivo. *Quant. Imaging Med. Surg.* 2012; 2(1): 1-11.
- Eskandari N, Yavari K, Outokesh M, Sadjadi S, Ahmadi SJ. Iodine-131 radiolabeling of poly ethylene glycol-coated gold nanorods for in vivo imaging. *J. Labelled Comp. Radiopharm.* 2013; 56(1): 12-6.
- Smith DK, Miller NR, Korgel BA. Iodide in CTAB prevents gold nanorod formation. *Langmuir.* 2009; 25(16): 9518-24.
- Su N, Dang Y, Liang G, Liu G. Iodine-125-labeled cRGD-gold nanoparticles as tumor-targeted radiosensitizer and imaging agent. *Nanoscale Res. Lett.* 2015; 10: 1.
- Shao X, Agarwal A, Rajian JR, Kotov NA, Wang X. Synthesis and bioevaluation of 125I-labeled gold nanorods. *Nanotechnology.* 2011; 22(13): 135102.
- Shao X, Zhang H, Rajian JR, Chamberland DL, Sherman PS, Quesada CA, et al. 125I-labeled gold nanorods for targeted imaging of inflammation. *ACS nano.* 2011; 5(11): 8967-73.
- Johnston Jr RB. Current concepts: immunology. Monocytes and macrophages. *N. Eng. J. Med.* 1988; 318(12): 747.
- Radhakrishnan R, Moore SA, Sluka KA. Unilateral carrageenan injection into muscle or joint induces chronic bilateral hyperalgesia in rats. *Pain.* 2003; 104(3): 567-77.
- Stumpe KD, Dazzi H, Schaffner A, von Schulthess GK. Infection imaging using whole-body FDG-PET. *Eur. J. Nucl. Med. Mol. Imaging.* 2000; 27(7): 822-32.
- Ren P-G, Lee S-W, Biswal S, Goodman SB. Systemic trafficking of macrophages induced by bone cement particles in nude mice. *Biomaterials.* 2008; 29(36): 4760-5.
- Wattanani S, Tornero D, Graubardt N, Memanishvili T, Monni E, Tatarishvili J, et al. Monocyte-derived macrophages contribute to spontaneous long-term functional recovery after stroke in mice. *J. Neurosci.* 2016; 36(15): 4182-95.
- Yang YH, Morand EF, Getting SJ, Paul-Clark M, Liu DL, Yona S, et al. Modulation of inflammation and response to dexamethasone by Annexin 1 in antigen-induced arthritis. *Arthritis Rheum.* 2004; 50(3): 976-84.
- Tremblay AM, Giguère V. The NR3B subgroup: an ovERRview. *Nucl. Recept. Signal.* 2007; 30(5): e009.
- Kim D-K, Gang G-T, Ryu D, Koh M, Kim Y-N, Kim SS, et al. Inverse agonist of nuclear receptor ERRγ mediates anti-diabetic effect through inhibition of hepatic gluconeogenesis. *Diabetes.* 2013; 62(9): 3093-102.
- Kim D-K, Jeong J-H, Lee J-M, Kim KS, Park S-H, Kim YD, et al. Inverse agonist of estrogen-related receptor [γ] controls Salmonella typhimurium infection by modulating host iron homeostasis. *Nat. Med.* 2014; 20(4): 419-24.